Journal of Glaciology



Article

Cite this article: Edasi SH and Lipovsky BP (2026) Tidewater and lake-terminating glaciers are systematically thicker. *Journal of Glaciology* **72**, e28, 1–8. https://doi.org/10.1017/jog.2026.10123

Received: 12 June 2025
Revised: 19 December 2025
Accepted: 8 January 2026

Keywords:
glacier modeling; glacier volume; ice/ocean interactions

Corresponding author:
Bradley Paul Lipovsky;
Email: bpl7@uw.edu

© The Author(s), 2026. Published by Cambridge University Press on behalf of International Glaciological Society. This is an Open Access article, distributed under the terms of the Creative Commons Attribution licence (http://creativecommons.org/licenses/by/4.0), which permits unrestricted re-use, distribution and reproduction, provided the original article is properly cited.

cambridge.org/jog

Tidewater and lake-terminating glaciers are systematically thicker

Simon Hans Edasi and Bradley Paul Lipovsky

Department of Earth & Space Sciences, University of Washington, Seattle, WA, USA

Abstract

Glaciers that terminate in the ocean or lakes exhibit unique dynamics that can drive rapid change. These dynamics, governed by many complex and interacting processes, challenge calibration and validation of physics-based models. We take a data-driven approach to quantify the imprint of glacier–ocean interactions on global non-ice sheet glacier ice volumes. Using curated datasets, we build a hierarchy of models that capture the influence of ice shelves and grounded marine termini. We find that tidewater and lake-terminating glaciers are systematically thicker than glaciers ending on land. Summed globally, this effect accounts for about 20% of non–ice-sheet glacier volume. Thicker ice is observed both for glaciers with ice shelves, where buttressing supports upstream ice, and for water-terminating glaciers without shelves. We interpret this result in terms of a simple mechanical model whereby water pressure permits thicker termini than possible in air, consistent with theoretical limits on ice cliff height. Our results highlight how ice–ocean interactions shape the equilibrium geometry of glaciers, offering a large-scale complement to process-based studies of calving and frontal melt. While most global glacier models omit these interactions, our analysis motivates their inclusion in forecasts of glacier change and sea level rise.

1. Introduction

Glaciers contribute significantly to sea level rise, with global glacier volume projected to decline by roughly 44% by 2100, equivalent to 19 cm of mean sea level rise 9-28 cm 90% confidence range; Fox-Kemper and others (2021). Although smaller in magnitude than the long-term contribution from ice sheets, glacier retreat plays a crucial role over the shorter time horizons most relevant to climate mitigation and adaptation (Glavovic and others, 2021). Glacier mass loss also drives acute local hazards, including slope failures, glacier collapses and outburst floods (Carrivick and Tweed, 2016; Kääb and others, 2018; Shugar and others, 2021; Svennevig and others, 2024).

Among glaciers, those that terminate in water—whether in the ocean (tidewater glaciers) or in proglacial lakes—stand out for their dynamism. For brevity, we refer to these collectively as *water-terminating glaciers*. Tidewater glaciers can undergo rapid cycles of advance and retreat (Meier and Post, 1987; O'Neel and others, 2005), while lake-terminating glaciers experience substantial subaqueous melt (Zhang and others, 2023). Much research has focused on process-level dynamics: calving laws (Vieli and others, 2001; Nick and others, 2010; Sergienko, 2022), mélange buttressing (Amundson and others, 2010) and submarine melt (Sutherland and others, 2019; Gräff and others, 2025). These studies have illuminated key mechanisms but leave open the broader question of how such processes shape the mean state of glaciers worldwide. Furthermore, most global-scale glacier models do not explicitly represent ice–ocean interactions, focusing instead on surface mass balance and simplified flow dynamics (Marzeion and others, 2020). This omission limits their ability to capture the distinct geometry and volume of water-terminating glaciers.

Here, we ask a simple but revealing question: 'for otherwise similar glaciers, are water-terminating glaciers on average thicker than their land-terminating counterparts?' This perspective highlights the role of the ice front as a boundary condition on glacier flow (van der Veen, 1996), where processes acting over small spatial and temporal scales collectively determine the large-scale equilibrium state. Calving dynamics, frontal melting, mélange buttressing and subaqueous melt each influence terminus mass and force balance, but their effects propagate far upstream through the force balance of the glacier. Theoretical studies have shown how calving laws can alter grounding line stability and the overall mass balance of marine-terminating glaciers (e.g., Schoof and others, 2017), underscoring the principle that localized physics at the terminus can reshape glacier-wide geometry. Our analysis captures this integrated outcome in the form of a shifted mean state: water-terminating glaciers tend to occupy a larger equilibrium geometry than their land-terminating counterparts, consistent with the additional support provided by water pressure at the ice front (Bassis and Walker, 2012).

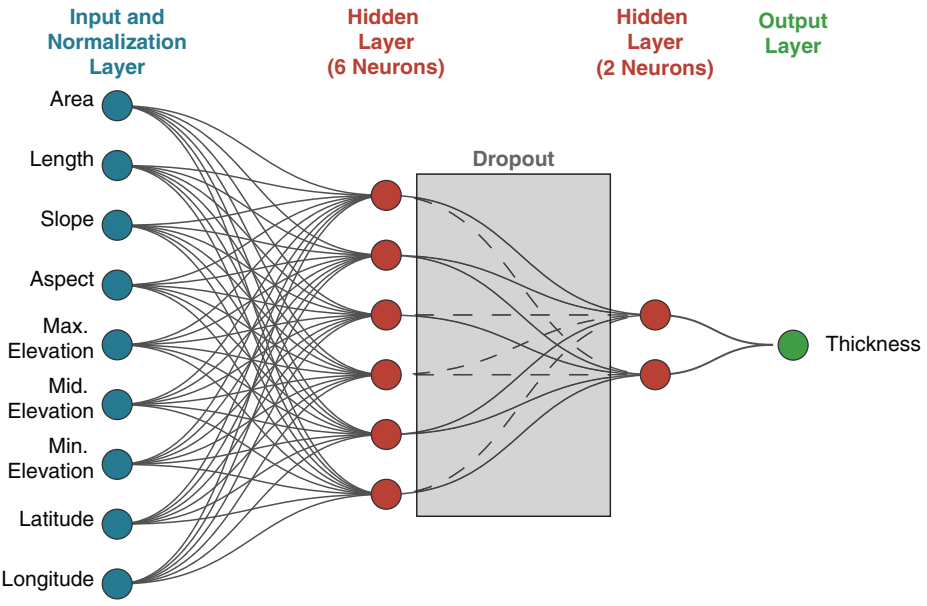


Figure 1. Our simple machine learning architecture features eleven inputs, normalization, two dense layers and a dropout layer.

By quantifying how this difference in mean state contributes to global ice volume, our data-driven approach complements process-based studies. We undertake a comprehensive uncertainty analysis (Section 3.4). The novelty of our approach is that we specifically exclude any water-terminating or ice shelf-supported glaciers in our training data. In this way, we derive a simple machine learning model that estimates glacier thicknesses in the absence of any glacier–ocean or glacier–lake interactions.

2. Data

This project uses two different datasets. The first dataset we use is the GlaThiDa database version 3.1.0 (Welty and others, 2020). From this dataset, we extract the labels (dependent variables) for our analysis, specifically, glacier thickness and thickness uncertainty. GlaThiDa contains three separate datasets that describe different scales of measurement. We use only the 'T' dataset that contains glacier-averaged thicknesses, i.e., each data point represents the average thickness over an entire glacier. There are $n = 500$ unique glaciers in this dataset.

The second dataset we use is the Randolph Glacier Inventory, Version 6 (Arendt and others, 2017). From this dataset, we extract the features (independent variables) for our analysis. This feature vector has a dimensionality of six, and consists of glacier centroid latitude, centroid longitude, area, slope, elevation and maximum length. Later, we will also use the terminus type feature from the RGI dataset, although this information is not incorporated into our regression analysis. Unlike the GlaThiDa dataset, the RGI dataset is globally complete ($n = 216501$).

3. Methods

The main goal of our approach is to carry out a regression analysis that estimates the average thickness of individual glaciers given a set of glacier-scale features (maximum length, average slope, etc.). We accomplish this regression using a shallow neural network (SNN; see Figure 1 and Methods). We first train the SNN on the small number of glaciers for which we have *in situ* thickness information, and we then apply the model to the globally-complete RGI database. In this section, we describe in detail the workflow required to achieve this goal.

3.1. Dataset coregistration

To combine glacier thickness observations from GlaThiDa with glacier outlines and attributes from the RGI, we must coregistered the two datasets so that each thickness measurement is paired with the correct glacier in the global inventory. Glaciers between the GlaThiDa and RGI catalogs are coregistered by finding the RGI glacier that is spatially closest to each GlaThiDa glacier. Although simple in principle, several complications occur in practice:

(1) Variable resolution of centroid coordinates in GlaThiDa sometimes introduces an ambiguity where several RGI glaciers may have numerical identical distances from a given GlaThiDa glacier or where one RGI glacier may have a numerically identical distance to several GlaThiDa glaciers. These cases are resolved by dropping the corresponding GlaThiDa glacier.
(2) Since years or decades may have passed between the epoch of the GlaThiDa and RGI measurements, there may not exist a well-defined match between the two catalogs. After matching by centroid location (as described above) a percent difference in size between entries in RGI and GlaThiDa is calculated as

$$\Delta A_i = \frac{A^{\mathrm{RGI}}_{k(i)} - A^{\mathrm{GlaThiDa}}_{i}}{A^{\mathrm{GlaThiDa}}_{i}}. \quad (1)$$

This equation introduces the notation where indices i and k to refer to glaciers in the GlaThiDa and RGI catalogs, respectively. Coregistration involves determining the mapping between the two indices, i.e., $k(i)$.

Equation 1 expresses the percent difference that represents changes in glacier surface area since thickness surveys were carried out and estimates the reliability of the available thickness data. ΔA_i can also be compared to a threshold of

https://doi.org/10.1017/jog.2026.10123 Published online by Cambridge University Press

uncertainty to dismiss any glaciers that may have unreliable labeled thickness for their measured size.

(3) A small number of coregistered glaciers are found to occur over an unrealistically large distance. To quantify this effect, the ratio $D = \frac{\Delta x}{r}$ is employed to compare the geometric glacier radius $r = \sqrt{\frac{A^{\mathrm{RGI}}}{\pi}}$, to the distance between catalogued glacier centroids, Δx. Threshold T is then introduced to exclude erroneous coregistrations. Four thresholds are tested ($T = 999, 0.75, 0.5, 0.25$) to find the ideal balance between sample size and reliability for training. These thresholds result in 400, 273, 202 and 105 labels, respectively. We discuss threshold selection below, after describing our shallow neural network (SNN) approach

3.2. Shallow neural networks (SNNs)

We carry out our regression analysis using a Shallow Neural Network (SNN; Figure 1). Our model is a two-hidden-layer multilayer perceptron (MLP) with ReLU activations, and a dropout rate of 0.1 between the hidden layers for regularization. Inputs are standardized with a Keras preprocessing. Normalization layer (used as the first layer). This layer is fitted on the training features only and performs per-feature z-score normalization (mean 0, unit variance). We train with early stopping on the validation loss, using a patience of 10 epochs and a minimum improvement of 0.001, restoring the best weights. Training runs up to 500 epochs but halts when the validation loss plateaus under these criteria, with these criteria being chosen to avoid overfitting.

With the goal of simplifying the parameters of the model, shallow neural networks (SNNs) with two layers of neurons are utilized. The network architecture consists of 6 neurons in the first layer and 2 neurons in the second layer surrounding a 10% dropout normalization layer to help prevent over-fitting (Srivastava and others, 2014). We tested a wide range of architectures by varying the number of neurons in each of the two hidden layers; however, we found that this had minimal impact on our results and we do not further investigate this aspect of our model here. Learning rate and validation split (for early stopping) are held fixed at 0.01 and 0.2, respectively. Model residuals for the i^{th} GlaThiDa glacier are calculated as

$$r_i = \hat{h}_i - h_i, \tag{2}$$

and fractional residual

$$R_i = \frac{\hat{h}_i - h_i}{h_i}, \tag{3}$$

where h_i is the observed (GlaThiDa-reported) glacier thickness, and $\hat{h}_i$ is the corresponding estimated thickness. Model weights are calculated by minimizing mean absolute error (MAE), $\sum_{i=1}^{N_{\mathrm{GlaThiDa}}} |r_i| / N_{\mathrm{GlaThiDa}}$, and mean squared error (MSE) $\sum_{i=1}^{N_{\mathrm{GlaThiDa}}} r_i^2 / N_{\mathrm{GlaThiDa}}$, where N_{GlaThiDa} is the number of glaciers in the GlaThiDa catalog. MAE describes how the model performs in estimating the average glacier, while MSE is more sensitive to larger errors which allows for discrimination against outliers.

3.3. Coregistration threshold selection

Although a strict coregistration threshold results matching glacier measurements more accurately, it also trades off against regression quality because fewer points are used. We quantify this tradeoff by examining model residuals (Equation 3) as a function of the threshold T (Figure S3). $T = 999$ represents all data regardless of area or location mismatch. This model does not perform well and estimates appear to hover around a mean value. $T = 0.25$ has very poor performance suggesting insufficient data for training. $T = 0.50$ and $T = 0.75$ estimates show improved performance. $T = 0.75$ is selected as the best fit to the data for further analysis.

3.4. Glacier volume and volume uncertainty calculation

For each of the $n = 216501$ glaciers in the RGI catalog indexed by k, glacier volume is calculated as the product $\hat{V}_k = \hat{H}_k \hat{A}_k$ (no summation on the index k) of the estimated thickness $\hat{H}_k$ and area $\hat{A}_k$. We begin by analyzing the area $\hat{A}_k$ and thickness $\hat{H}_k$ terms separately, in Sections 3.4.1 and 3.4.2, before combining them to analyze volume in Section 3.4.3.

3.4.1. Glacier area and area uncertainty

The estimated area $\hat{A}_k$ consists of the RGI-reported area A_k, which is modeled as a normal distribution,

$$\hat{A}_k \sim \mathcal{N}\left[A_k, \mathrm{Var}\left(A_k\right)\right]. \tag{4}$$

Uncertainties due to mapping errors are quantified following the result of Pfeffer and others (2014), who estimated area uncertainty with a simple model of fitting a curve to fractional uncertainties between multiple data sources for RGI. Their approximation yields the relationship

$$\mathrm{Var}\left(A_k\right) \approx c_1 \alpha \left(A_k^{p_1}\right)^2, \tag{5}$$

where A_k is the reported glacier surface area, $\alpha = 0.039$ is the estimated fractional error of a 1 km^2 glacier and $p_1 = 0.70$ and $c_1 = 3$ are empirical constants fit from by Pfeffer and others (2014).

3.4.2. Glacier thickness and thickness uncertainty

To estimate the mean thickness of each glacier, we adopted a leave-one-out (LOO) cross-validation strategy rather than the more common 70/30 train/test split. In a typical 70/30 split, only a single partition of the data is withheld for testing, which can be limiting when the dataset is small. Because our coregistered database contains relatively few glaciers, we were able to apply the more detailed LOO approach: for each target glacier k, we retrained the model while leaving out each of the other $N = 272$ glaciers one at a time. This produces a full distribution of predictions that captures the sensitivity of glacier k's estimate to every other glacier in the dataset. In this way, our LOO design both guards against overfitting and makes the most of limited data by ensuring that every glacier is tested repeatedly under slightly different training conditions.

Formally, the estimated thickness $\hat{H}_k$ of glacier k is modeled as a normal distribution centered on the ensemble mean thickness H_k with variance reflecting the spread of predictions across LOO iterations,

$$\hat{H}_k \sim \mathcal{N}\left[H_k, \mathrm{Var}\left(H_k\right)\right]. \tag{6}$$

For each LOO run, denoted $\mathcal{H}_{kj}$, we predict the thickness of glacier k using a regression trained on the entire GlaThiDa database

https://doi.org/10.1017/jog.2026.10123 Published online by Cambridge University Press

except for glacier j. Averaging over all such runs yields the expected value of the thickness,

$$H_k = \frac{1}{N_j}\sum_{j=1}^{N_j}\mathcal{H}_{kj}, \tag{7}$$

where $N_j = 273$ is the number of cross-validation iterations. In this way, every glacier is both excluded once for testing and included many times for training, ensuring that the final thickness estimates reflect out-of-sample predictive performance.

Thickness uncertainty $\mathrm{Var}\left(H_k\right)$ results from three sources: underlying measurement uncertainty $\mathrm{Var}\left(\epsilon_k^{\mathcal{M}}\right)$, uncertainty due to limited thickness data $\mathrm{Var}\left(\epsilon_k^{\mathcal{H}}\right)$ and model uncertainty $\mathrm{Var}\left(\epsilon_k^{\mathcal{R}}\right)$:

$$\mathrm{Var}\left(H_k\right) = \mathrm{Var}\left(\epsilon_k^{\mathcal{M}}\right) + \mathrm{Var}\left(\epsilon_k^{\mathcal{H}}\right) + \mathrm{Var}\left(\epsilon_k^{\mathcal{R}}\right). \tag{8}$$

We analyze each of the contributions to Equation 8 individually.

The first contribution to thickness uncertainty, reliability of training data, is assessed by approximating the measurement uncertainty of data used for training, $\mathrm{Var}\left(\epsilon^{\mathcal{M}}\right)$. This uncertainty is approximated by fitting a curve to the thickness uncertainty data provided by the GlaThiDa dataset as a function of glacier thickness. The resulting empirical curve is

$$\sqrt{\mathrm{Var}\left(\epsilon_i^{\mathcal{M}}\right)} \approx c_2 h_i^{p_2}, \tag{9}$$

with empirically determined constants $c_2 \approx 0.07$ and $p_2 \approx 0.8$. This model is then used to approximate the effect of measurement uncertainty, $\mathrm{Var}\left(\epsilon_k^{\mathcal{M}}\right)$, using H_k as the dependent variable.

The second contribution to thickness uncertainty, uncertainty due to limited thickness data $\mathrm{Var}\left(\epsilon_k^{\mathcal{H}}\right)$, is quantified using leave one out cross validation. The variance over the cross validation iterations is given by

$$\mathrm{Var}\left(\epsilon_k^{\mathcal{H}}\right) \approx \mathrm{Var}_j\left(\mathcal{H}_{kj}\right). \tag{10}$$

Here, the notation $\mathrm{Var}(\cdot)$ is used to denote the variance of a random variable and the notation $\mathrm{Var}_j(\cdot)$ to denote the statistical operation of taking the variance of an array of values.

The third contribution to thickness uncertainty, the neural network regression model uncertainty $\mathrm{Var}\left(\epsilon_k^{\mathcal{R}}\right)$, is approximated by analyzing model residuals. A statistical model of residuals is calculated by binning similar thickness estimates h_i into $B < n_i$ bins. Then, for each of the ℓ bins, $0 < \ell \leq B$, the standard deviation of pooled residuals r_{jB} is calculated as

$$\sqrt{\mathrm{Var}\left(\epsilon_\ell^{\mathcal{R}}\right)} \approx \sqrt{\frac{1}{Bn_j}\sum_{\ell}^{B}\sum_{j}^{n_j}\left(r_{j\ell} - \bar{r}_\ell\right)^2}. \tag{11}$$

Due to limited thickness data, some bins must be expanded such that at least 3 glaciers are included to calculate $\mathrm{Var}\left(\epsilon_B^{\mathcal{R}}\right)$. These standard deviations are then fit as a dependent variable to binned thickness measurement h_ℓ in log-log space, which yields the power law relationship

$$\sqrt{\mathrm{Var}\left(\epsilon_B^{\mathcal{R}}\right)} \approx c_3 h_B^{p_3}, \tag{12}$$

with constants $c_3 = 0.04$ and $p_3 = 0.6$. This power law statistical model is then used to estimate $\mathrm{Var}\left(\epsilon_k^{\mathcal{R}}\right)$ using H_k as the dependent variable. This approach is similar to the one employed by Farinotti and others (2019), hereafter, F19, i.e., their expression '$1.5\sigma_i/\bar{h}_i$', with the additional generalization that F19 essentially assumed a power law exponent of one, whereas we fit an exponent from the data. The covariance terms between uncertainties are calculated to be at least two orders of magnitude smaller than the other terms and so they are neglected going forward.

3.4.3. Individual and global glacier volume and associated uncertainty

With these distributions in hand, glacier volume variance can be calculated on a glacier-by-glacier basis for all glaciers in the RGI catalog. For the time being, it is assumed that $\hat{H}_k$ and $\hat{A}_k$ are uncorrelated. In that case, the variance of the k^{th} glacier is calculated as

$$\begin{aligned}\sigma_k^2 &= \mathrm{Var}(\hat{H}_k\hat{A}_k)\\ &= \mathrm{Var}\left(\hat{H}_k\right)\mathrm{Var}\left(\hat{A}_k\right) + A_k^2\mathrm{Var}\left(\hat{H}_k\right) + H_k^2\mathrm{Var}\left(\hat{A}_k\right),\end{aligned} \tag{13}$$

where we do not sum over repeated indices.

The sum global volume is considered a random variable with a sampling distribution defined by estimated parameters,

$$\hat{S} \sim \mathcal{N}\left(\sum_k^{N_k}\hat{V}_k, \sum_k^{N_k}\sigma_k^2\right). \tag{14}$$

The sum global volume is approximated as

$$S \approx \sum_{k=1}^{N_k}\hat{V}_k \pm Z^*_{\alpha/2}\sqrt{\sum_k^{N_k}\sigma_k^2}. \tag{15}$$

4. Results

4.1. Global analysis

When we train an SNN to estimate global glacier volumes, but exclude any glaciers that terminate in an ice shelf, the resulting model predicts a global glacier volume $136 \pm 2 \times 10^3$ km^3. Our model performs nearly identically to the physics-based multi-model voting scheme of Farinotti and others (2019), hereafter, F19 in terms of cross validation performance in the training dataset: our model has a thickness residual of -3 ± 28 m (mean $\pm$ standard deviation) compared to 3 ± 33 m for the F19 model (Figure S1). However, the global ice volume estimate from our model is significantly lower than the estimate of F19, who found a global glacier volume of $158 \pm 16 \times 10^3$ km^3 (see discussion of uncertainties, below). Our model therefore predicts $22 \pm 16 \times 10^3$ km^3 less ice volume globally. If we further exclude all ocean- and lake-terminating glaciers from the training data set, our global ice volume estimate further decreases to $126.1 \pm 3.3 \times 10^3$ km^3, a difference of $32 \pm 16 \times 10^3$ km^3. This discrepancy is globally significant; it is nominally (i.e., neglecting buoyancy effects of partially submerged ice) equivalent to 6.2 cm of sea level rise.

We interpret this difference as being due to the inadequate representation of water-terminating glaciers in our training dataset. The difference is due to a small number of glaciers: 70% of the difference between these models is explained by only 0.4% of glaciers in the RGI database (about 1000 individual glaciers). Of the 100 most negative volume differences, 42 are marine-terminating ice caps and 40 are ice shelf-supported glaciers near the Antarctic ice sheet. Regional variations, shown in Figure 2, show that our model exhibits the most significant negative biases in the Antarctic/Subantarctic (RGI region 19), the North Canadian Arctic (RGI region 2), Iceland (RGI region 6), Svalbard and Jan Mayen (RGI region 7) and the Russian Arctic (RGI region 9).

Our model makes comparable predictions to previously published global glacier volume estimates for glaciers that are not lake–terminating or ocean–terminating. Figure 3 compares our glacier volume estimates to those of F19 and Millan and others (2022), hereafter 'M22' for all glaciers in the RGI database. Our

https://doi.org/10.1017/jog.2026.10123 Published online by Cambridge University Press

Region	Farinotti et al. 2019 (10^3 km^3)	Millan et al. 2022 (10^3 km^3)	This Study (10^3 km^3)
1 Alaska	18.98 +/- 4.92	* +/- *	19.91 +/- 1.65
2 Western Canada and US	1.06 +/- 0.27	* +/- *	0.83 +/- 0.06
3 North Canadian Arctic	28.33 +/- 7.35	25.4 +/- 7.2	21.6 +/- 1.32
4 South Canadian Arctic	8.61 +/- 2.23	7.0 +/- 2.1	5.3 +/- 0.5
5 Greenland Periphery	15.69 +/- 4.07	11.8 +/- 3.7	25.21 +/- 3.0
6 Iceland	3.77 +/- 0.98	3.7 +/- 0.9	2.38 +/- 0.38
7 Svalbard and Jan Mayen	7.47 +/- 1.94	7.0 +/- 2.3	5.49 +/- 0.37
8 Scandinavia	0.3 +/- 0.08	0.29 +/- 0.1	0.18 +/- 0.01
9 Russian Arctic	14.64 +/- 3.8	15.5 +/- 3.9	7.88 +/- 0.5
10 North Asia	0.14 +/- 0.04	0.09 +/- 0.05	0.16 +/- 0.01
11 Central Europe	0.13 +/- 0.03	0.12 +/- 0.05	0.1 +/- 0.01
12 Caucus and Middle East	0.06 +/- 0.02	0.06 +/- 0.03	0.06 +/- 0.005
13 Central Asia	3.27 +/- 0.85	* +/- *	3.34 +/- 0.15
14 South West Asia	2.87 +/- 0.74	* +/- *	3.18 +/- 0.3
15 South East Asia	0.88 +/- 0.23	* +/- *	0.91 +/- 0.03
16 Low Latitudes	0.1 +/- 0.03	0.07 +/- 0.04	0.06 +/- 0.003
17 Southern Andes	5.34 +/- 1.39	5.9 +/- 1.6	4.42 +/- 0.4
18 New Zealand	0.07 +/- 0.02	0.07 +/- 0.03	0.09 +/- 0.01
19 Antarctic and Subantarctic	46.47 +/- 12.06	35.1 +/- 9.1	34.55 +/- 3.11

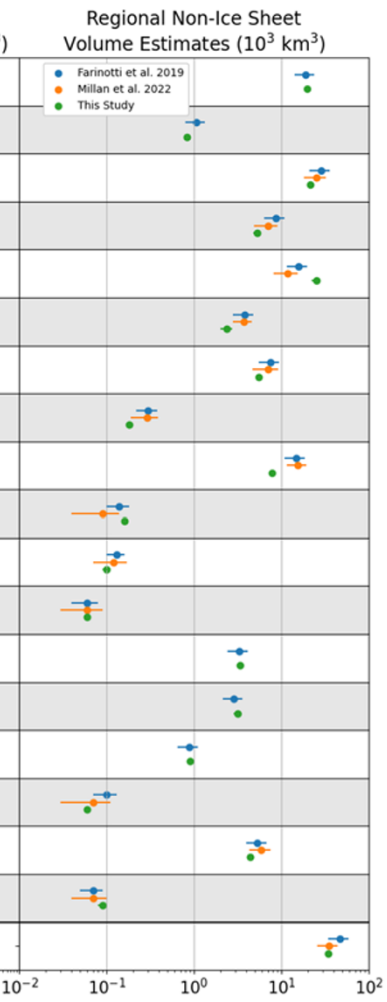


Figure 2. RGI regional volume comparisons between F19, M22 and this study. M22 combined Alaska and Western Canada (RGI 1, 2, respectively) into a single region, as well as high-mountain Asia (RGI regions 13,14,15) into a single region making it not possible to compare these regions. Discrepancies with M22 occur due to differing glacier domains (as noted by Hock and others, 2023). Comparisons with the underlying data are shown in the Supplementary Information.

results are also similar in the distribution of glacier sizes, where we find that 67% of the global glacier volume is contained in just 0.2% of the world's glaciers (377 individual glaciers). Small glaciers with estimated volumes < 0.1 km^3 show a slight positive difference in our model compared to F19, while volumes > 0.1 km^3 show a slight negative difference compared to F19. Our model estimates regional glacier volumes that are largely within the confidence intervals of previous studies in regions with few water-terminating glaciers (Figure 2). We note that a handful of glaciers in Jan Mayen were estimated by F19 to be on the order of centimeters thick, which is interpreted as an artifact in that model (Figure 3).

4.2. Uncertainty quantification

We carry out a comprehensive analysis of sources of uncertainty in our calculations and find that the global glacier volume uncertainty σ^2 can be approximated as, $\sigma^2 \approx A_k^2 \mathrm{Var}\left(\hat{H}_k\right)$, where the index k refers to a particular glacier (with summation implied by the repeated indices), A_k refers to the area of that glacier and $\hat{H}_k$ refers to its estimated thickness. The full expansion for σ is given in the Methods.

Our analysis shows that global glacier volume uncertainty is predominantly controlled by glacier thickness rather than area (Methods). Of the terms that contribute to thickness uncertainty, we find that limited thickness observations are the dominant source of uncertainty (54% of the variance), followed by underlying measurement uncertainty (35%) and model misfit (11%). All other terms account for less than 0.05% of the variance. A statistical summary of these results is given in Figure S2 and Table S6.

On a glacier-by-glacier basis, we find that thickness uncertainty for the smallest glaciers can vary between 35% and 55%. Percent uncertainty decreases with increasing glacier size to roughly 10% for the largest glaciers. These results are presented graphically in Figure S4.

When comparing the confidence intervals between our study and F19, it is important to note that F19 used a heuristic approach to calculating these confidence intervals from regional uncertainty estimates. Specifically, F19 calculated their global confidence intervals as the sum of the standard deviations, rather than the sum of variances. While this approach results in a larger and more conservative uncertainty estimate, it does not preserve linearity for independent measurements. As a result, we note that F19 presented wider confidence intervals of $\pm 41 \times 10^3$ km^3 rather than the value

https://doi.org/10.1017/jog.2026.10123 Published online by Cambridge University Press

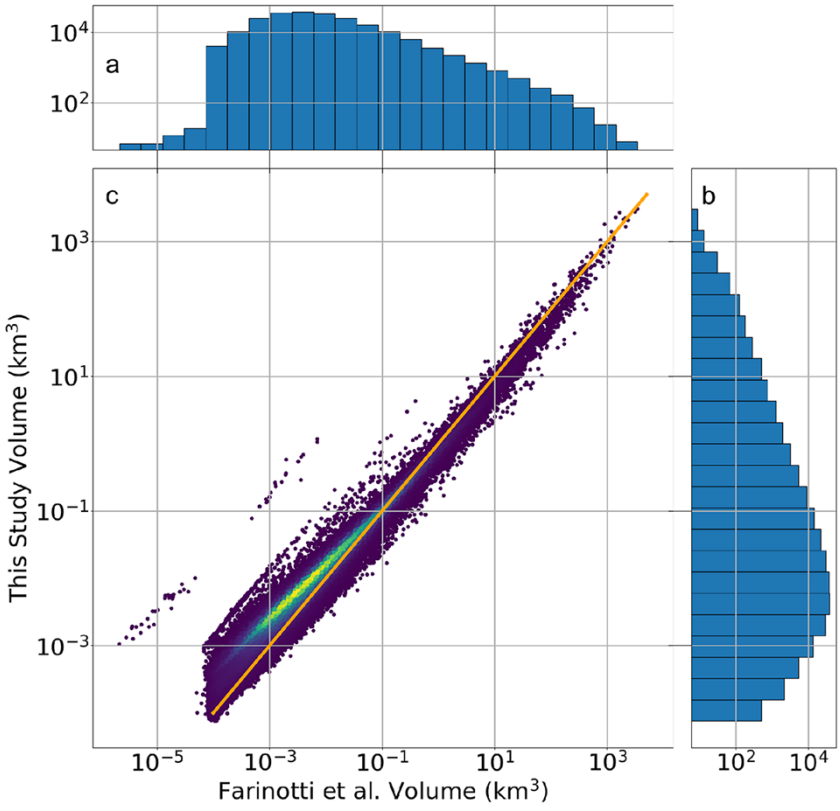


Figure 3. (a) Histogram of volumes from Farinotti et al. 2019. (b) Histogram of volumes from this study. (c) Direct global comparison between volumes estimated by this study and that of Farinotti et al. 2019 on a log scale with one-to-one perfect fit in orange. Brighter colors represent the density of estimates. Summary statistics for our glacier volume estimates are given in Tables S1–S5.

that we quote of $\pm 16 \times 10^3$ km^3 that arises from summing variances rather than standard deviations.

5. Discussion

Ice–ocean and ice–lake interactions are widely recognized as key controls on glacier dynamics, influencing calving rates, frontal melting and the force and mass balance at glacier termini (Benn and others, 2007). These processes are often observed to be sources of rapid change and potential instability, yet they also shape the equilibrium glacier geometry. In this study, we quantify the imprint of these interactions at the global scale by comparing models trained with and without water-terminating glaciers. We find that excluding ice–ocean and ice–lake interactions leads to a systematically lower estimate of global glacier volume, with the difference accounting for $20 \pm 10\%$ of the total non-ice sheet global glacier volume. This result is consistent with the well-established role of ice shelves in buttressing grounded ice and supporting greater ice volumes in marine ice sheet systems (Rignot and others, 2004; Dupont and Alley, 2005; Gudmundsson, 2013), but it also extends to water-terminating glaciers without ice shelves. Our findings therefore highlight that the presence of water at the ice front is a first-order control on the mean equilibrium state of glaciers.

Our conclusion that water-terminating glaciers are systematically thicker than land-terminating glaciers is consistent with both regional observations and theoretical considerations. In Svalbard, van Pelt and Frank (2025) found that glacier-averaged median thickness is about four times larger for tidewater glaciers (162 m) than for land-terminating glaciers (42 m). In High Mountain Asia, a population comparison indicates that lake-terminating glaciers are, on average, thicker over their ablation zones ($\sim$110 m vs. $\sim$100 m) and especially near their termini (Pronk and others, 2021), complementing earlier work that documented contrasting geometry, thinning and retreat patterns by terminus type (King and others, 2018). From an inversion perspective, neglecting frontal ablation systematically underestimates both mass turnover and near-front thickness for marine-terminating glaciers, inflating regional underestimation of stored ice by $\sim$11–19% (Recinos and others, 2019).

These empirical results align with height-above-buoyancy (HAB) considerations: water pressure at the ice front permits thicker termini than would be sustainable in air alone, setting a different boundary condition for equilibrium geometry (Nick and others, 2010; Bassis and Walker, 2012). Bassis and Walker (2012) argued that Coulomb plastic fracturing limits the heights of subaerial ice cliffs to a height $H_c \approx 100$ m. Glaciers that terminate on land must therefore have terminus thickness $H(0) < H_c$. Glaciers that terminate in water instead must have terminus thickness $H(0) < H_w + H_c$ where $H_w > 0$ is the water depth. To illustrate the implications of this boundary condition, we consider an idealized glacier profile $H(x) = \sqrt{2x\tau/(\rho g) + H(0)^2}$, with gravitational acceleration g and bed strength $\tau \approx 100$ kPa. Equipped with this model, we find that a 20 km long land-terminating glacier has an average thickness of 459 m, whereas a 20 km long ocean-terminating glacier has an average thickness of 610 m, a difference of 33%. While research has often emphasized the role of ice cliff failure in rapid ice mass loss (Pollard and others, 2015; DeConto and Pollard, 2016), our analysis highlights the complementary point that water pressure at the ice front also supports thicker equilibrium termini. In this way, processes that might destabilize glaciers at short timescales can simultaneously shift their mean state toward larger volumes.

https://doi.org/10.1017/jog.2026.10123 Published online by Cambridge University Press

Forecasting models of glacier mass loss most often neglect ice–ocean interactions that are thought to be important for larger marine ice sheets. In the ensemble of models described by Marzeion and others (2020), for example, only one out of eleven models attempted to include ice–ocean interactions. Recent progress in the field has begun to place more emphasis on these processes (Recinos and others, 2019; Malles and others, 2023; Rounce and others, 2023). As water-terminating glaciers retreat and evolve into land-terminating systems, models that do not capture ice–ocean and ice–lake interactions may have limited ability to represent this transition. Our analysis thus provides new evidence that the boundary conditions at glacier termini fundamentally shape equilibrium thickness, with consequences for global ice volume and its sensitivity to climate forcing.

Data availability statement. All code is available with download links to data on GitHub and published through Zenodo: https://zenodo.org/records/11106415.

Supplementary material. The supplementary material for this article can be found at https://doi.org/10.1017/jog.2026.10123.

Acknowledgements. This manuscript improved because of discussions with David Rounce and Nathan Kutz.

References

Amundson JM, Fahnestock M, Truffer M, Brown J, Lüthi MP and Motyka RJ (2010) Ice mélange dynamics and implications for terminus stability, Jakobshavn Isbræ, Greenland. *Journal of Geophysical Research: Earth Surface* **115**, F01005. doi: 10.1029/2009JF001405.

Arendt A and 11 others (2017) *Randolph Glacier Inventory - A Dataset of Global Glacier Outlines* Version 6. doi: 10.7265/4m1f-gd79.

Bassis JN and Walker CC (2012) Upper and lower limits on the stability of calving glaciers from the yield strength envelope of ice. *Proceedings of the Royal Society A: Mathematical, Physical and Engineering Sciences* **468**, 913–931. doi: 10.1098/rspa.2011.0422.

Benn DI, Warren CR and Mottram RH (2007) Calving processes and the dynamics of calving glaciers. *Earth-Science Reviews* **82**, 143–179. doi: 10.1016/j.earscirev.2007.02.002.

Carrivick JL and Tweed FS (2016) A global assessment of the societal impacts of glacier outburst floods. *Global and Planetary Change* **144**, 1–16. doi: 10.1016/j.gloplacha.2016.07.001.

DeConto RM and Pollard D (2016) Contribution of Antarctica to past and future sea-level rise. *Nature* **531**, 591–597. doi: 10.1038/nature17145.

Dupont T and Alley R (2005) Assessment of the importance of ice-shelf buttressing to ice-sheet flow. *Geophysical Research Letters* **32**, L04503. doi: 10.1029/2004GL022024.

Farinotti D and 6 others (2019) A consensus estimate for the ice thickness distribution of all glaciers on Earth. *Nature Geoscience* **12**, 168–173. doi: 10.1038/s41561-019-0300-3.

Fox-Kemper B and 17 others (2021) Ocean, cryosphere and sea level change. In Masson-Delmotte V et al. (eds.) *Climate Change 2021: The Physical Science Basis. Contribution of Working Group I to the Sixth Assessment Report of the Intergovernmental Panel on Climate Change*, Book Section 9, Cambridge University Press. doi:10.1017/9781009157896.011.

Glavovic B, Dawson R, Chow WT, Garschagen M, Singh C and Thomas A (2021) Cities and settlements by the sea. In Roberts D et al. (eds.) *Climate Change 2022: Impacts, Adaptation and Vulnerability. Contribution of Working Group II to the Sixth Assessment Report of the Intergovernmental Panel on Climate Change*, Cross-Chapter Paper 2, Cambridge University Press. doi:10.1017/9781009325844.019.

Gräff D and **10 others** (2025) Calving-driven fjord dynamics resolved by seafloor fibre sensing. *Nature* **644**, 404–412. doi: 10.1038/s41586-025-09347-7.

Gudmundsson G (2013) Ice-shelf buttressing and the stability of marine ice sheets. *The Cryosphere* **7**, 647–655. doi: 10.5194/tc-7-647-2013.

Hock R, Maussion F, Marzeion B and Nowicki S (2023) What is the global glacier ice volume outside the ice sheets? *Journal of Glaciology* **69**(273), 204–210. doi: 10.1017/jog.2023.1.

Kääb A and 10 others (2018) Massive collapse of two glaciers in western Tibet in 2016 after surge-like instability. *Nature Geoscience* **11**, 114–120. doi: 10.1038/s41561-017-0039-7.

King O, Dehecq A, Quincey D and Carrivick J (2018) Contrasting geometric and dynamic evolution of lake and land-terminating glaciers in the central Himalaya. *Global and Planetary Change* **167** 46–60. doi: 10.1016/j.gloplacha.2018.05.006.

Malles JH, Maussion F, Ultee L, Kochtitzky W, Copland L and Marzeion B (2023) Exploring the impact of a frontal ablation parameterization on projected 21st-century mass change for Northern Hemisphere glaciers. *Journal of Glaciology* **69**(277), 1317–1332. doi: 10.1017/jog.2023.19.

Marzeion B and 10 others (2020) Partitioning the uncertainty of ensemble projections of global glacier mass change. *Earth's Future* **8**, e2019EF001470. doi: 10.1029/2019EF001470.

Meier M and Post A (1987) Fast tidewater glaciers. *Journal of Geophysical Research: Solid Earth* **92**, 9051–9058. doi: 10.1029/JB092iB09p09051.

Millan R, Mouginot J, Rabatel A and Morlighem M (2022) Ice velocity and thickness of the world's glaciers. *Nature Geoscience* **15**, 124–129. doi: 10.1038/s41561—00885-z.

Nick F, van der Veen C, Vieli A and Benn D (2010) A physically based calving model applied to marine outlet glaciers and implications for the glacier dynamics. *Journal of Glaciology* **56**(199), 781–794. doi: 10.3189/002214310794457344.

O'Neel S, Pfeffer WT, Krimmel R and Meier M (2005) Evolving force balance at Columbia Glacier, Alaska, during its rapid retreat. *Journal of Geophysical Research: Earth Surface* **110**, F03012. doi: 10.1029/2005JF000292.

Pfeffer WT and 19 others (2014) The Randolph Glacier Inventory: a globally complete inventory of glaciers. *Journal of Glaciology* **60**(221), 537–552. doi: 10.3189/2014JoG13J176.

Pollard D, DeConto RM and Alley RB (2015) Potential Antarctic ice sheet retreat driven by hydrofracturing and ice cliff failure. *Earth and Planetary Science Letters* **412** 112–121. doi: 10.1016/j.jpgl.2014.12.035.

Pronk JB, Bolch T, King O, Wouters B and Benn DI (2021) Contrasting surface velocities between lake- and land-terminating glaciers in the Himalayan region. *The Cryosphere* **15** 5577–5599. doi: 10.5194/tc-15-5577-2021.

Recinos B, Maussion F, Rothenpieler T and Marzeion B (2019) Impact of frontal ablation on the ice thickness estimation of marine-terminating glaciers in Alaska. *The Cryosphere* **13**, 2657–2672. doi: 10.5194/tc-13-2657-2019.

Rignot E, Casassa G, Gogineni P, Krabill W, Rivera A and Thomas R (2004) Accelerated ice discharge from the Antarctic Peninsula following the collapse of Larsen B ice shelf. *Geophysical Research Letters* **31**, L18401. doi: 10.1029/2004GL020697.

Rounce DR and 10 others (2023) Global glacier change in the 21st century: every increase in temperature matters. *Science* **379**, 78–83. doi: 10.1126/science.abo1324.

Schoof C, Davis AD and Popa TV (2017) Boundary layer models for calving marine outlet glaciers. *The Cryosphere* **11**, 2283–2303. doi: 10.5194/tc-11-2283-2017.

Sergienko O (2022) Marine outlet glacier dynamics, steady states and steady-state stability. *Journal of Glaciology* **68**(271), 946–960. doi: 10.1017/jog.2022.13.

Shugar DH and 10 others (2021) A massive rock and ice avalanche caused the 2021 disaster at Chamoli, Indian Himalaya. *Science* **373**, 300–306. doi: 10.1126/science.abh4455.

Srivastava N, Hinton G, Krizhevsky A, Sutskever I and Salakhutdinov R (2014) Dropout: a simple way to prevent neural networks from overfitting. *The Journal of Machine Learning Research* **15**, 1929–1958. doi: 10.9734/ajrcos/2025/v18i2569.

Sutherland D and 8 others (2019) Direct observations of submarine melt and subsurface geometry at a tidewater glacier. *Science* **365**, 369–374. doi: 10.1126/science.aax3528.

Svennevig K and 10 others (2024) A rockslide-generated tsunami in a Greenland fjord rang Earth for 9 days. *Science* **385**, 1196–1205. doi: 10.1126/science.adm9247.

van der Veen C (1996) Tidewater calving. *Journal of Glaciology* **42**(141), 375–385. doi: 10.3189/S0022143000004226.

van Pelt W and Frank T (2025) New glacier thickness and bed topography maps for Svalbard. *The Cryosphere* **19**, 1–17. doi: 10.5194/tc-19-1-2025.

Vieli A, Funk M and Blatter H (2001) Flow dynamics of tidewater glaciers: a numerical modelling approach. *Journal of Glaciology* **47**(159), 595–606. doi: 10.3189/172756501781831747.

Welty E and 10 others (2020) Worldwide version-controlled database of glacier thickness observations. *Earth System Science Data Discussions* **2020** 1–27. doi: 10.5194/essd-12-3039-2020.

Zhang G and 9 others (2023) Underestimated mass loss from lake-terminating glaciers in the greater Himalaya. *Nature Geoscience* **16**, 333–338. doi: 10.1038/s41561-023-01150-1.

https://doi.org/10.1017/jog.2026.10123 Published online by Cambridge University Press